NANO LETTERS

pubs.acs.org/NanoLett Letter

Chiroptical Response of Aluminum Nanocrescents at Ultraviolet Wavelengths

Matthew S. Davis,* Wenqi Zhu, Jared Strait, Jay K. Lee, Henri J. Lezec, Steve Blair,* and Amit Agrawal*

Cite This: *Nano Lett.* 2020, 20, 3656−3662 Read Online

ACCESS | Metrics & More | Article Recommendations

ABSTRACT: Manipulation of plasmon modes at ultraviolet wavelengths using engineered nanophotonic devices allows for the development of high-sensitivity chiroptical spectroscopy systems. We present here an experimental framework based on aluminum-based crescent-shaped nanostructures that exhibit a strong chiroptical response at ultraviolet wavelengths. Through utilization of higher-order plasmon modes in wavelength-scale nanostructures, we address the inherent fabrication challenges in scaling the response to higher frequencies. Additionally, the distinct far-field spectral response types are analyzed within a coupled-oscillator model framework. We find two competing chiroptical response types that contribute toward potential ambiguity in the interpretation of the circular dichroism spectra. The first, optical activity, originates from the interaction between hybridized eigenmodes, whereas the second manifests as a response superficially similar to optical activity but originating instead from differential near-field absorption modes. The study of the chiroptical response from nanoplasmonic devices presented here is expected to aid the development of next-generation chiroptical spectroscopy systems.

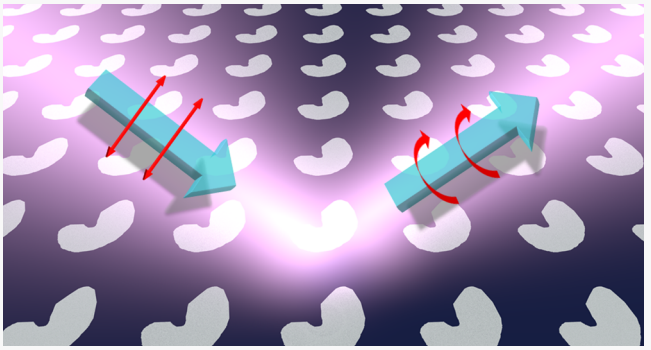

KEYWORDS: *chirality/optical activity, UV−vis spectroscopy, metals, molecular modeling*

INTRODUCTION

Engineered nanostructures with plasmon resonances at ultraviolet (UV) wavelengths have enabled the development of applications such as deep-UV surface-enhanced Raman spectroscopy[1] and optoelectronics with wide-bandgap materials.[2] Additionally, dielectric and plasmon-enhanced circular dichroism (CD) spectroscopy has been shown to strengthen the naturally weak coupling between circularly polarized (CP) light and biomolecular resonances at UV wavelengths by up to 3 orders of magnitude,[3−7] suggesting enhanced spectroscopy tools that will directly impact the development of pharmaceuticals,[8−10] the characterization of protein secondary structures and folding,[11] and the treatment of diseases.[12] The fabrication challenges inherent to scaling these engineered structures for enhanced UV applications are overcome through the manipulation of tunable higher-order resonances in optically large nanostructures,[7,13] indicating a method for implementing UV-interactive nanostructures for enhanced CD spectroscopy applications. However, the presence of optically large engineered nanostructures constituting an optical medium can contribute to ambiguity in the resulting CD measurements.[14,15] A robust framework is therefore required to correctly extract information relevant to optical activity from a CD spectrum.

CD spectroscopic measurements in typical commercial systems are obtained by subtracting the transmission/reflection of right and left CP light (RCP and LCP, respectively) through/from a molecular system. This far-field differential transmission/reflection measurement is not necessarily related to CD, however, and so is instead referred to here as the chiroptical (CO) response, where CO = $T_{RCP} - T_{LCP}$, and T_{RCP} (T_{LCP}) is the transmitted intensity upon illumination with RCP (LCP) light.[14] A CO measurement may indicate the presence of optical activity in a molecular substrate, where optical activity is produced by the differential excitation of hybridized eigenmodes in molecular or plasmonic structures.[16] The corresponding far-field CO response originating from optical activity is referred to here as CO_{OA}. However, ambiguity in a CO measurement can result from the presence of anisotropy either in a natural molecular system or artificially introduced with plasmonic structures.[17] The CO response of anisotropic media has been

Received: February 10, 2020
Revised: April 7, 2020
Published: April 21, 2020

https://dx.doi.org/10.1021/acs.nanolett.0c00586
Nano Lett. 2020, 20, 3656−3662

shown to result from the differential near-field absorption modes generating a far-field CO response that is unrelated to optical activity. This response type is referred to here as CO_{abs}, with the total chiroptical response expressed as $CO = CO_{OA} + CO_{abs}$. Due to the presence of these competing response types in an optical medium, the analysis and interpretation of a CO measurement typically requires the extraction of the full Mueller matrix;[15,18] however, previous work demonstrated an alternative method for distinguishing between CO_{OA} and CO_{abs} using only the differential transmission (reflection) measurement.[14]

Here, we present a novel nanophotonic platform based on an array of wavelength scale aluminum (Al) nanocrescents exhibiting a strong CO response at UV wavelengths, and furthermore, we utilize a coupled-oscillator-based analytical model for identifying the presence of, and distinguishing between, CO_{OA} and CO_{abs} in measured CO spectra. An *N*-coupled-oscillator model suitable for describing higher-order plasmonic modes at UV wavelengths is shown here to replicate the subtle and salient features of the measured CO spectra over a range of source orientations. The *N*-oscillator model serves as a computationally simple tool for interpreting and intuitively understanding the physical origins of the relatively easy-to-implement CO spectroscopic measurement of complicated plasmonic nanostructures, thus facilitating the design of structures appropriate for plasmon-enhanced CD spectroscopic applications.

FABRICATION AND EXPERIMENTAL RESULTS

Excitation of plasmon modes with molecular resonances in the UV presents design and fabrication challenges due to limitations of the resolution of lithographic techniques and selection of the constituent materials. The manipulation of higher-order plasmonic modes has been proposed as a solution to the fabrication resolution issue as these modes can be accessed with ease in structures that are not deeply subwavelength.[7,13] Plasmonic systems have been previously shown to exhibit strong CO responses in the UV range[19] and has required exploration of nontraditional plasmonic metals such as Al, gallium, magnesium, and rhodium.[20−22] Al is an abundant and inexpensive material featuring strong plasmon resonances in the deep-UV range. Despite the red-shifting and weakening of the plasmon resonances caused by a naturally self-terminating 3 nm thick oxide layer,[7,23−25] Al remains a viable option for UV plasmonic applications. The field-dampening effects can further be mitigated through the manipulation of higher-order mode excitations, and therefore, the crescent-shaped nanostructures presented in this work are able to couple efficiently to UV plasmonic modes. Additionally, the crescent shapes are geometrically chiral, thus directly inducing a CP selectivity for the excited modes.

The crescents are fabricated on 500 μm thick fused-silica substrates. A 100 nm thick poly(methyl methacrylate) (PMMA) resist is spin-coated on the substrates, followed by deposition of 20 nm Al film (anticharging layer) using thermal evaporation. This is followed by electron-beam lithography at 100 keV. The Al layer is then removed using a 60 s bath in a tetramethylammonium−hydroxide-based developer followed by a 30 s rinse in deionized water. PMMA is developed for 90 s in methyl isobutyl ketone followed by a 30 s rinse in isopropyl alcohol. A 40 nm thick Al film is then deposited using electron beam evaporation. The final step is a 12 h soak in acetone for lift-off. Al crescent structures, each with a maximum structural feature size of 220 nm, are arrayed in a periodic square lattice with pitch of 325 nm, covering a total area of 500 μm × 500 μm (Figure 1a).

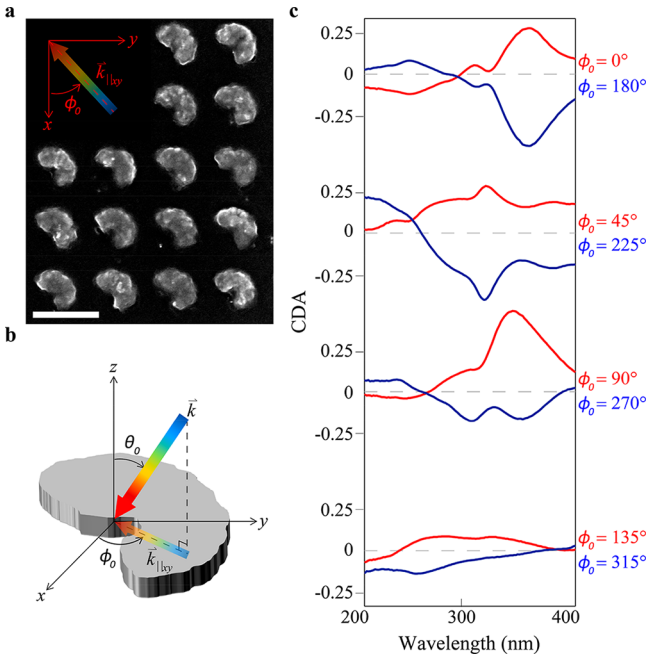

Figure 1. Circular diattenuation (CDA) spectra of Al crescent structures at UV wavelengths. (a) Scanning electron microscopy image of the Al crescent structures aligned in a square periodic array with a pitch of 325 nm. The white bar inset represents 325 nm. The additional inset illustrates the in-plane coordinate system used for describing the measurements in c. (b) Out-of-plane coordinate system detailing how CDA spectra are obtained in reflection mode by illuminating the Al structures with angled light. (c) Experimental CDA measurements of Al crescent structure array illuminated with free-space light of wavelengths ranging from 200 to 400 nm at an incident angle of $\theta_0 = 45°$ and various ϕ_0 angles.

The CO response of the crescent structure array is characterized using a broadband UV source (wavelengths 200−400 nm, beam diameter ≈ 350 μm), illuminating at a fixed inclination angle of $\theta_0 = 45°$ and varying azimuth angle ϕ_0 (Figure 1b). The measured normalized CO spectra, referred to here as circular diattenuation (CDA) and expressed as $CDA = (T_{RCP} - T_{LCP})/(T_{RCP} + T_{LCP})$, is shown in Figure 1c. The CDA spectra are measured by extracting the m_{14} element of the Mueller matrix using spectroscopic ellipsometry in the reflection mode.[26] The CDA spectra measured here display a clear azimuthal dependence. Notably, when the source is rotated azimuthally by 180°, the CDA amplitude experiences an inversion in sign about the vertical axis. This amplitude sign flip has been previously observed in planar plasmonic structures by oblique light illumination.[14] The CDA spectra further show asymmetric amplitude inversion accompanying the sign flip. This is most prominent in the CDA spectra for $\phi_0 = 90$ and 270°. Note that the substrate does not play any role in the observed CDA spectra as a function of azimuthal angle.[14−17,27−29] As described in the next section, these spectral characteristics indicate the simultaneous presence of CO_{OA} and CO_{abs} in the system.

https://dx.doi.org/10.1021/acs.nanolett.0c00586
Nano Lett. 2020, 20, 3656−3662

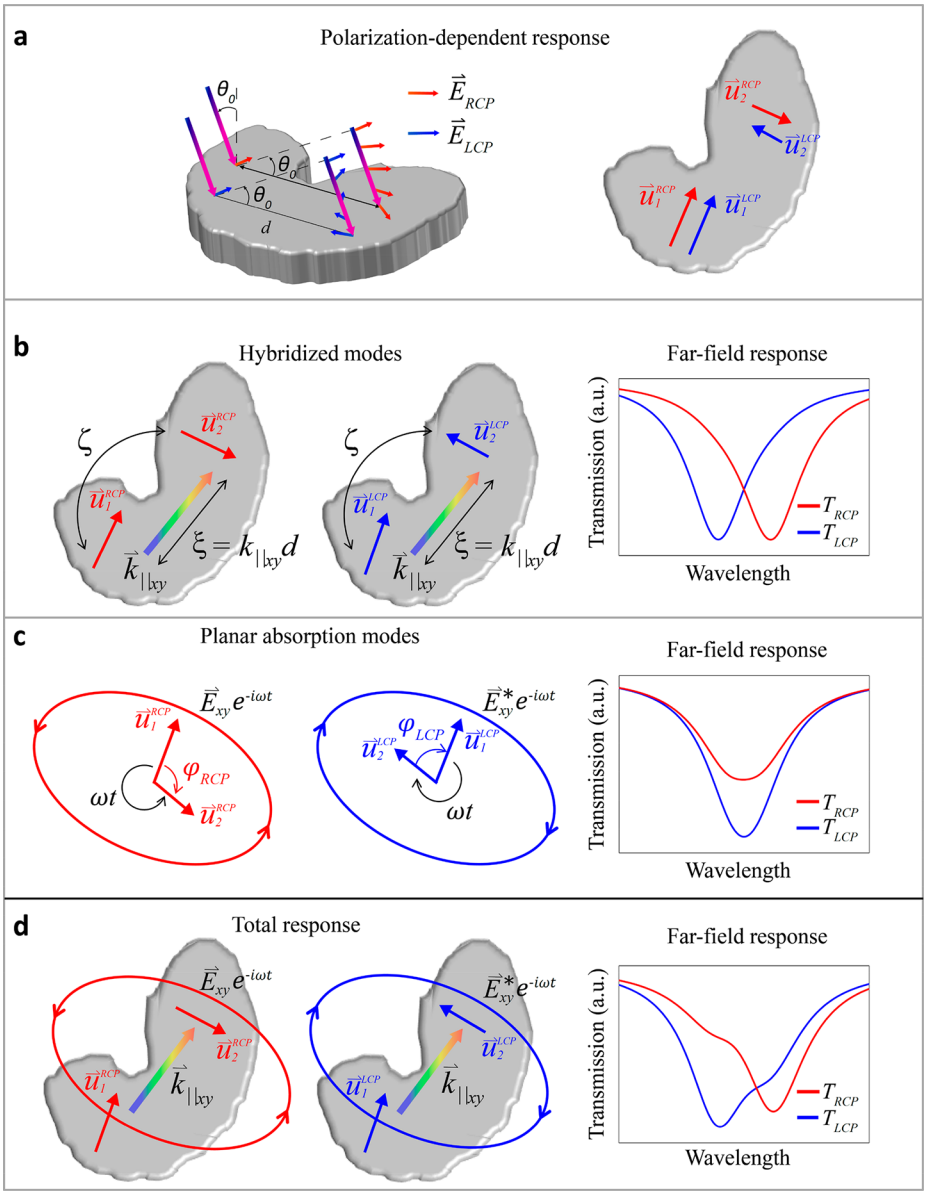

Figure 2. Origins of the chiroptical response of an optically large structure. (a) Source field is incident on the Al crescent-shaped structure. The orientation of the electric field varies along the surface of the structure, resulting in a polarization-dependent mode excitation (represented by two coupled oscillators). The excitation of each oscillator for a RCP (LCP) source field is described by $\vec{u}_k^{\,\mathrm{RCP}} = \vec{E}_0 \cdot \hat{u}_k e^{i\xi_k}$ ($\vec{u}_k^{\,\mathrm{LCP}} = \vec{E}_0^{\,*} \cdot u_k e^{i\xi_k}$ where $\xi_k = \vec{k} \cdot \vec{r}_k$ and $k = 1, 2$. Both $\vec{u}_k^{\,\mathrm{RCP}}$ and $\vec{u}_k^{\,\mathrm{LCP}}$ are generally not equivalent, and therefore, a nonzero CO response may be observed. Additionally, each oscillator $\vec{u}_k$ produces a far-field transmission peak centered around its resonance frequency ω_k for integer k. In this example, the two oscillators, $\vec{u}_1$ and $\vec{u}_2$, are shown with resonance frequencies, ω_1 and ω_2, selected close enough to each other such that the combined far-field response appears as a single spread out transmission peak. (b) A system of coupled oscillators separated by some distance d along the direction of source propagation can produce nondegenerate hybridized modes resulting in red and blue-shifted transmission spectra for RCP and LCP light, respectively (or vice versa). (c) The $\mathrm{CO_{abs}}$ response type originates from the far-field interaction of radiating dipoles. A polarization-dependent phase difference creates transmission spectra for RCP and LCP source fields that are shifted in amplitude relative to each other. (d) The CO response of a plasmonic structure results from the simultaneous contributions of the $\mathrm{CO_{OA}}$ and $\mathrm{CO_{abs}}$ responses. The transmission spectra of the two-oscillator system for RCP and LCP light is both shifted in wavelength and amplitude. The total CO response exhibits wavelength and amplitude asymmetries consistent with those experimentally observed in the Al crescent structures.

■ ANALYSIS OF THE CO RESPONSE

A simple method for describing the characteristics of the CO response is to replace the localized surface plasmon modes of the crescent structures with a system of two coupled oscillators, $\vec{u}_1$ and $\vec{u}_2$, with amplitudes given by $u_k = \vec{E}_0 \cdot \hat{u}_k e^{i\xi_k}$, where $\xi_k = \vec{k} \cdot \vec{r}_k$.

Figure 2a shows the surface variation in the field component of a CP source incident at angle θ_0 on a crescent plasmonic structure. The excited modes in the oscillator model depend on both source polarization and oscillator orientation for RCP and LCP source fields (Figure 2b). Two CP excitation modes are possible for a given source orientation, with one mode described by the

https://dx.doi.org/10.1021/acs.nanolett.0c00586
Nano Lett. 2020, 20, 3656−3662

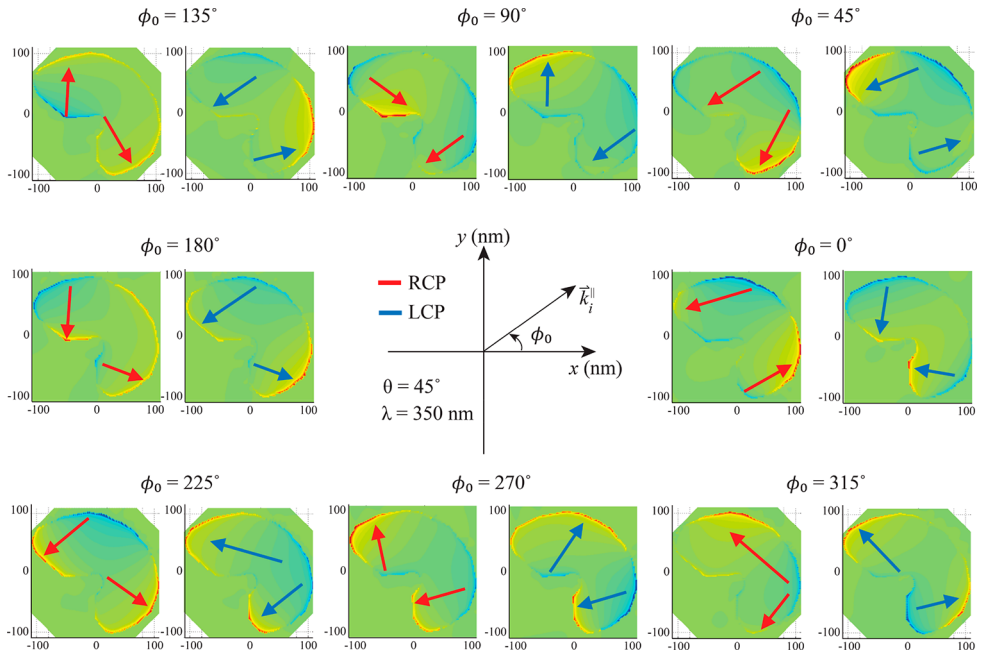

Figure 3. Evolution of near-field mode distribution. Near-field mode distributions, calculated using the finite-difference time-domain technique, for an individual nanocrescent at wavelength of $\lambda = 350$ nm, incident inclination angle of $\theta_0 = 45°$, and various azimuthal angles ϕ_0. The red and blue colors of the arrows indicate RCP and LCP illumination, respectively, and the arrows qualitatively indicate the orientation of the two lower-order dipole modes within the nanostructure.

set of excitations ($\vec{u}_1^{\,\mathrm{RCP}}$, $\vec{u}_2^{\,\mathrm{RCP}}$) and the other by ($\vec{u}_1^{\,\mathrm{LCP}}$, $\vec{u}_2^{\,\mathrm{LCP}}$). The corresponding near-field mode distributions, calculated using the finite-difference time-domain (FDTD) technique, along with the oscillator orientations for an individual nanocrescent at the resonance wavelength of $\lambda = 350$ nm and incident angle of $\theta_0 = 45°$ for various ϕ_0 angles considered in this study, are shown in Figure 3. For each azimuth angle, two arrows representing oscillators are superimposed onto the crescent structure, where each arrow is oriented to point from a negative (blue) to a positive (red) near-field region as calculated using FDTD simulations. A two-oscillator model has previously been shown to accurately simulate the far-field response of subwavelength nanorod structures,[14] and the depiction in Figure 3 suggests that two oscillators may also approximately simulate the modal behavior of the optically large crescent structures. Further insight may be gained into the CO response of the crescent structures by considering the far-field CO response calculated by only considering two oscillators.

The far-field response of an oscillator system is a result of the presence of hybridized[16] and absorption[28] modes. To illustrate the hybridized modes, consider that $\vec{u}_1$ and $\vec{u}_2$ are separated by distance d along the direction of source propagation in the $x-y$ plane (Figure 2b). The coupled two-oscillator system exhibits RCP ($\vec{u}_1^{\,\mathrm{RCP}}$, $\vec{u}_2^{\,\mathrm{RCP}}$) and LCP ($\vec{u}_1^{\,\mathrm{LCP}}$, $\vec{u}_2^{\,\mathrm{LCP}}$) hybridized modes, one blue-shifted in wavelength relative to the other. This CO response is characterized in the far-field by blue and red-shifted transmission (or reflection) spectra and is indicative of optical activity. This response type is referred to as $\mathrm{CO_{OA}}$ and has been previously shown to obey the relationship:[14,28]

$$\mathrm{CO_{OA}} \propto \zeta \sin(k_{\parallel xy} d) \tag{1}$$

where d is the separation distance between the two oscillators in the direction of wavevector $\vec{k}_{\parallel xy}$, and ζ represents the electromagnetic coupling between the pair of oscillators. Note that, according to eq 1, $\mathrm{CO_{OA}}$ must change sign if the source azimuth flips 180°. This behavior originates from the physical separation along the direction of source propagation of coupled oscillators and is consistent with the measured spectra of the crescent structures (Figure 1c).

The oscillator excitations may also exhibit absorption modes with each oscillator acting as an independently radiating dipole (Figure 2c). The far-field radiative fields interfere either constructively or destructively in a manner that depends on both the polarization state of the source fields and relative orientation of the oscillators. The interference results in transmission peaks aligned in wavelength but with differing amplitude peaks. This type of CO response is referred to as $\mathrm{CO_{abs}}$ and is characterized by amplitude shifted transmission (reflection) spectra. $\mathrm{CO_{abs}}$ is indicative of anisotropy and has been shown to obey the relationship[14,29]

$$\mathrm{CO_{abs}} \propto \omega\gamma(\omega_1^2 - \omega_2^2)\sin\varphi\cos\varphi \tag{2}$$

where ω is the source frequeqncy, ω_1 (ω_2) is the resonance frequency of oscillator 1 (2), φ is the angular separation between the oscillators, and γ is the damping coefficient. Equation 2 implies that two oscillators oriented either parallel or perpendicular to each other will not produce a $\mathrm{CO_{abs}}$ response. Note also that according to eq 2, $\mathrm{CO_{abs}}$ does not change sign as the source azimuthally rotates.

The total chiroptical response of the two-oscillator system is given by $\mathrm{CO} = \mathrm{CO_{OA}} + \mathrm{CO_{abs}}$. The wavelength and amplitude shifted transmission spectra of the two-oscillator system for RCP and LCP light are shown in Figure 2d. These equations describe several spectral features observed in the measured spectra obtained from the crescent structures (Figure 1c). For example, the CO spectra invert asymmetrically in amplitude because the $\mathrm{CO_{OA}}$ component changes sign with a 180° source azimuthal rotation, but amplitude asymmetry is observed in the total

https://dx.doi.org/10.1021/acs.nanolett.0c00586
Nano Lett. 2020, 20, 3656−3662

response because the CO_{abs} component is independent of source azimuth angle. The presence of both amplitude flipping and asymmetry in the measured spectra indicates the simultaneous presence of both optical activity and anisotropy. However, the presentation of each in a far-field measurement is strongly dependent on the source orientation. For example, as indicated by eq 1, the CO_{OA} contribution will go to zero for a source field normally incident on the planar Al crescent structures, as the in-plane oscillators will no longer be separated along the direction of source propagation. In general, however, the total CO response does not necessarily approach zero for normally incident light. From eq 2, it is evident that CO_{abs} is not dependent on $k_{\parallel xy}$ and is therefore nonzero at normal incidence. The presence of this type of CO response, which is not circular dichroism, for normally incident light has been observed in several other works.[14,27−29] As illustrated in Figure 2, the two-oscillator model described by eqs 1 and 2 provides an intuitively simple explanation for the origins of the far-field spectral profile of a CO response. This model is successful at reproducing and describing the origins of the azimuthally varying amplitude sign inversions that are clearly manifested in the measured CO response of the crescent structures in Figure 1.

Although the two-oscillator model captures many of the spectral features observed in the measured CO response, the spectral data exhibit multiple peaks which are indicative of higher-order plasmon modes that manifest because the nanocrescent structures are not deeply subwavelength. The two-oscillator model is therefore not suitable to simulate the far-field response of structures that exhibit such higher-order modes, as evident from the nonideal fit between the measured and calculated CDA spectra (Figure 4a). Furthermore, the most prominent observed spectral peak is source dependent and, as an example, shifts from $\lambda = 350$ nm at $\phi_0 = 0°$ to $\lambda = 325$ nm at $\phi_0 = 45°$. This behavior cannot be captured by a simple approximation of the system using a two-oscillator model. We overcome this shortcoming by extending the model from two to N oscillators, where N is a positive integer.

N-COUPLED-OSCILLATOR MODEL

Equations 1 and 2 describe many, but not all of, the observed spectral features in Figure 4a. An extension to N oscillators is required to adequately characterize the measured CO spectra, where $N \geq 2$. A system of N lossy coupled electron oscillators, located and oriented arbitrarily, can represent the higher-order mode excitations present at UV wavelengths, and this system is described by[30]

$$\partial_t^2 \vec{u_k} + \gamma_k \partial_t \vec{u_k} + \omega_k^2 \vec{u_k} + \hat{u}_k \sum_{n \neq k} \zeta_{n,k} u_n = -\frac{e}{m^*}(\vec{E_0}\cdot\hat{u}_k)\hat{u}_k e^{i(\vec{k}\cdot\vec{r_k} - \omega t)} \quad (3)$$

where $n, k = 1, 2, ..., N$. Each oscillator is characterized by a charge e, an effective mass m^*, an amplitude oscillation u_k, orientation $\hat{u}_k$, location $\vec{r_k}$, resonant frequency ω_k, and a damping factor γ_k. The electromagnetic coupling between any two oscillators u_n and u_k is given by the coefficient $\zeta_{n,k}$. Furthermore, the system of oscillators is excited by an incident planar source $\vec{E_0} e^{i\left(\vec{k}\cdot\vec{r} - \omega t\right)}$ with frequency ω, wavevector $\vec{k}$, and amplitude $\vec{E_0}$. Inserting time harmonic expressions $\vec{u_k} = \hat{u}_k u_k e^{-i\omega t}$ reduces eq 3 to

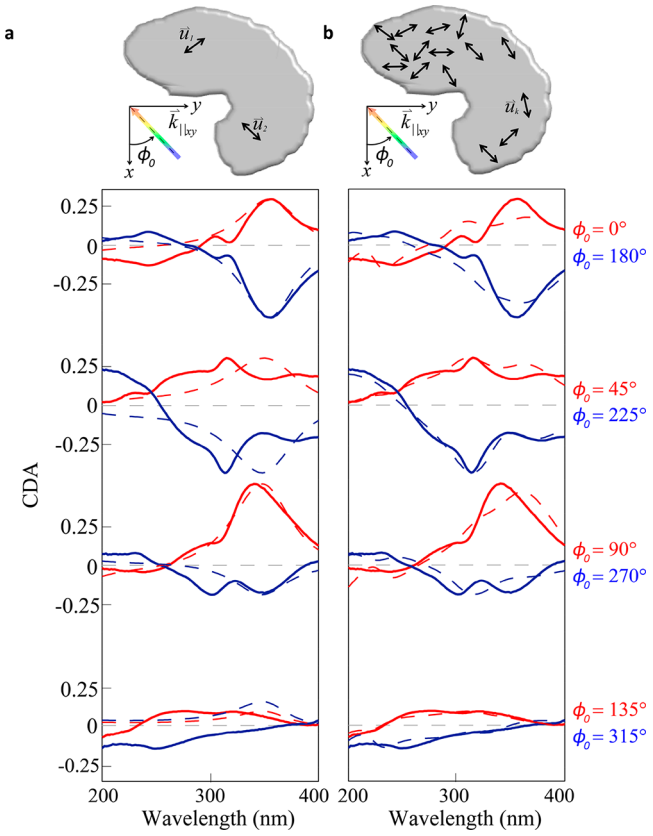

Figure 4. Model fit with N oscillators. (a) Fitting measured spectra (solid lines) using eq 9 with $N = 2$ oscillators (dashed lines). $N = 2$ oscillators are sufficient to describe the single-mode resonance behavior observed in the CDA spectra near $\lambda = 350$ nm but are unable to reproduce the additional spectral features observed at shorter wavelengths and at different source azimuthal angles. Note the mismatch in model prediction to measured spectra for $\phi_0 = 45°$ or $\phi_0 = 225°$. The most prominent spectral peak is dependent on the source azimuth, and this feature cannot be modeled with a two-oscillator system. (b) Fitting measured spectra (solid lines) using eq 9 with $N = 15$ oscillators (dashed lines). Using $N = 15$ oscillators more accurately reproduces these additional spectral features over the entire spectral range and also over the full range of source azimuthal angles.

$$[(\omega_k^2 - \omega^2) - i\gamma_k\omega]u_k + \sum_{n \neq k} \zeta_{n,k} u_n = -\frac{e}{m^*}(\vec{E_0}\cdot\hat{u}_k)e^{i\vec{k}\cdot(\vec{r_0} + \delta\vec{r_k})} \quad (4)$$

where $\vec{r_k} = \vec{r_0} + \delta\vec{r_k}$, with $\delta\vec{r_k}$ being the distance of oscillator k from the location of the structure center-of-mass $\vec{r_0}$ as defined in ref 5. Equation 4 can then be rewritten in the matrix form as

$$\begin{pmatrix} (\omega_1^2 - \omega^2) - i\gamma_1\omega & \cdots & \zeta_{1,N} \\ \vdots & \ddots & \vdots \\ \zeta_{N,1} & \cdots & (\omega_N^2 - \omega^2) - i\gamma_N\omega \end{pmatrix} \begin{pmatrix} u_1 \\ \vdots \\ u_N \end{pmatrix} = -\frac{e}{m^*} \begin{pmatrix} e^{i\vec{k}\cdot(\vec{r_0} + \delta\vec{r_1})} & \cdots & 0 \\ \vdots & \ddots & \vdots \\ 0 & \cdots & e^{i\vec{k}\cdot(\vec{r_0} + \delta\vec{r_N})} \end{pmatrix} \begin{pmatrix} E_1 \\ \vdots \\ E_N \end{pmatrix} \quad (5)$$

https://dx.doi.org/10.1021/acs.nanolett.0c00586
Nano Lett. 2020, 20, 3656−3662

with source field components $E_k = \vec{E_0}\cdot\hat{u}_k$ for $k = 1, 2, ..., N$. This expression is written more compactly as

$$\mathbf{\Omega}\vec{U} = -\frac{e}{m^*}\mathbf{K}\vec{E} \tag{6}$$

The matrix $\mathbf{\Omega}$ has diagonal elements $\Omega_{k,k} = (\omega_k^2 - \omega^2) - i\gamma_k\omega$ and off-diagonal elements $\Omega_{n,k} = \zeta_{n,k}$. The matrix $\mathbf{K}$ has elements $K_{n,k} = \delta_{n,k}e^{i\vec{k}\cdot\left(\vec{r}_0+\vec{\delta r}_k\right)}$, where $\delta_{n,k}$ is the Kronecker delta. Further defining the matrix $\mathbf{\Lambda} = \mathbf{\Omega}^{-1}\mathbf{K}$ gives a compact solution for the amplitude oscillations as

$$\vec{U} = -\frac{e}{m^*}\mathbf{\Lambda}\vec{E} \tag{7}$$

Each component u_n of $\vec{U}$ represents the amplitude oscillation of the nth oscillator. The current density response for the collection of excited oscillators is then calculated as

$$\vec{J} = -i\omega\varepsilon_0\omega_p^2\sum_k \hat{u}_k(\mathbf{\Lambda}\vec{E})_{k\,\vec{r}_0=\vec{r}-\vec{\delta r}_k} \tag{8}$$

Finally, the CO response of the oscillator system is

$$\mathrm{CO} = |\vec{J}_{\mathrm{RCP}}|^2 - |\vec{J}_{\mathrm{LCP}}|^2 \tag{9}$$

where $\vec{J}_{\mathrm{RCP}}$ ($\vec{J}_{\mathrm{LCP}}$) is calculated from eq 8 using a circularly polarized source field amplitude $\vec{E}_0$ ($\vec{E}_0^*$).

The CO spectra are calculated from eq 9 using a least-squares-fitting algorithm to select appropriate oscillator parameters defined in eq 3 in order to reproduce the measured CDA response. The parameter space was initialized with $\gamma_k = 1 \times 10^{15}$ s^{-1} and $\zeta_{n,k} = 1 \times 10^{15}$ s^{-2}. Additionally, the oscillators are initially randomly placed and orientated within the $x-y$ plane boundary defined by the optical structure and a resonance wavelength between 200 and 400 nm is assigned for each oscillator. The algorithm gradually optimizes these initialized parameters in order to improve the match between the calculated and the measured spectrum, computing successive generations of solutions and minimizing the difference between calculation and measurement until no significant improvement is observed. The algorithm used for this study does not guarantee avoidance of local minima, and therefore, the result is not claimed as a unique or even optimal solution; however as discussed below, even without knowledge of the near-fields, the oscillator system chosen by the algorithm successfully replicates the observed far-field CDA spectra of the crescent shaped structures because it is able to adequately simulate the sophisticated distribution of hybridized and absorption modes present in a multioscillator system.

Additionally, the placement of each oscillator relative to the others is not arbitrary. Similar to eq 1, the electromagnetic coupling between all oscillators contribute to the $\mathrm{CO_{OA}}$ response. This relative phase shift between each oscillator pair $k_{\|xy}d_{n,k}$ is azimuthally dependent; therefore, the $\mathrm{CO_{OA}}$ response is expected to become minimal at azimuthal orientations where the relative phase shifts are small. The measured CDA of the crescent structures approaches zero when $\phi_0 = 135$ and 315°; this is due to the average oscillator phase shifts along the direction of source propagation becoming a minimum at these azimuth angles. A geometric interpretation is that at $\phi_0 = 135°$ the crescent structure no longer appears chiral (or only weakly so) to the incident light. Furthermore, in agreement with eq 9, the absorption modes contributing to the observed amplitude asymmetry are dependent only on the relative orientations and resonant frequencies of each oscillator, thus the resulting far-field response does not change sign as the excitation source azimuthal angle is flipped by 180°. This $\mathrm{CO_{abs}}$ response is unrelated to circular dichroism and optical activity, and unlike $\mathrm{CO_{OA}}$, two-dimensional planar structures can still produce a nonzero CO response as $\theta_0 \to 0°$. The agreement with measurement is significantly improved from the simple two-oscillator calculation if $N = 15$ oscillators are used, as shown in Figure 4b. The calculated spectra now match many of the spectral peaks observed in the measurements, namely, peaks at $\lambda = 350$ nm for $\phi_0 = 0$ and 180°, $\lambda = 314$ nm for $\phi_0 = 45$ and 225°, and $\lambda = 300$ nm for $\phi_0 = 90$ and 270°. The number of oscillators, $N = 15$, was determined through the trade-off between computational resources and model-fit accuracy.

CONCLUSION

In summary, we experimentally characterize the chiroptical response of Al crescent shaped structures at UV wavelengths and analytically describe the measurements within the framework of a coupled-oscillator system. This model uses a set of N oscillators to represent higher-order plasmon mode excitations, and was shown to reproduce the salient features of the measured CDA spectra. The calculated spectra suggest contributions from both $\mathrm{CO_{OA}}$ and $\mathrm{CO_{abs}}$, indicating the presence of optical activity and anisotropy in the crescent structures at non-normal incident source angles. To summarize, the $\mathrm{CO_{OA}}$ response is related to optical activity and originates from hybridized modes in the multioscillator system, as described by the model. This response type is characterized in the far-field by wavelength shifted transmission curves. The model also predicts that a $\mathrm{CO_{abs}}$ response is characterized in the far-field by a shifting in amplitude between RCP and LCP light, and is indicative of anisotropy. Without the need for extensive experimental setups required for a full Mueller matrix spectroscopy, the model given by eq 3 is shown to serve as a useful tool for the interpretation of easy-to-implement transmission (reflection) CDA measurements at UV wavelengths of complex plasmonic nanostructures.

AUTHOR INFORMATION

Corresponding Authors

Matthew S. Davis − *National Institute of Standards and Technology, Gaithersburg, Maryland 20899, United States; Maryland NanoCenter, University of Maryland, College Park, Maryland 20742, United States; Department of Electrical Engineering and Computer Science, Syracuse University, Syracuse, New York 13244, United States*; Email: msdavi01@syr.edu

Steve Blair − *Department of Electrical and Computer Engineering, University of Utah, Salt Lake City, Utah 84112, United States*; orcid.org/0000-0001-5784-590X; Email: blair@ece.utah.edu

Amit Agrawal − *National Institute of Standards and Technology, Gaithersburg, Maryland 20899, United States; Maryland NanoCenter, University of Maryland, College Park, Maryland 20742, United States*; orcid.org/0000-0002-9619-7623; Email: amit.agrawal@nist.gov

Authors

Wenqi Zhu − *National Institute of Standards and Technology, Gaithersburg, Maryland 20899, United States; Maryland*

https://dx.doi.org/10.1021/acs.nanolett.0c00586
Nano Lett. 2020, 20, 3656−3662

NanoCenter, University of Maryland, College Park, Maryland 20742, United States

Jared Strait − *National Institute of Standards and Technology, Gaithersburg, Maryland 20899, United States*

Jay K. Lee − *Department of Electrical Engineering and Computer Science, Syracuse University, Syracuse, New York 13244, United States*

Henri J. Lezec − *National Institute of Standards and Technology, Gaithersburg, Maryland 20899, United States;* orcid.org/0000-0002-9808-1333

Complete contact information is available at: https://pubs.acs.org/10.1021/acs.nanolett.0c00586

Notes

The authors declare no competing financial interest.

■ ACKNOWLEDGMENTS

M.S.D., W.Z., and A.A. acknowledge support under the Cooperative Research Agreement between the University of Maryland and the National Institute of Standards and Technology, Physical Measurement Laboratory, Award No. 70NANB14H209, through the University of Maryland. S.B. acknowledges support from the NSF MRSEC program at the University of Utah under Grant No. DMR-1121252 and partial support from the ECCS Division of NSF (Award 1810096).

■ REFERENCES

(1) Dörfer, T.; Schmitt, M.; Popp, J. Deep-UV surface-enhanced Raman scattering. *J. Raman Spectrosc.* **2007**, *38*, 1379.

(2) Okamoto, K.; Niki, I.; Shvartser, A.; Narukawa, Y.; Mukai, T.; Scherer, A. Surface-plasmon-enhanced light emitters based on InGaN quantum wells. *Nat. Mater.* **2004**, *3*, 601.

(3) Abdulrahman, N.; Fan, Z.; Tonooka, T.; Kelly, S.; Gadegaard, N.; Hendry, E.; Govorov, A. O.; Kadodwala, M. Induced chirality through electromagnetic coupling between chiral molecular layers and plasmonic nanostructures. *Nano Lett.* **2012**, *12*, 977.

(4) Nesterov, M. L.; Yin, X.; Schäferling, M.; Giessen, H.; Weiss, T. The role of plasmon-generated near fields for enhanced circular dichroism spectroscopy. *ACS Photonics* **2016**, *3*, 578.

(5) Ben-Moshe, A.; Maoz, B. M.; Govorov, A. O.; Markovich, G. Chirality and chiroptical effects in inorganic nanocrystal systems with plasmon and exciton resonances. *Chem. Soc. Rev.* **2013**, *42*, 7028.

(6) Hu, J.; Lawrence, M.; Dionne, J. A. High quality factor dielectric metasurfaces for ultraviolet circular dichroism spectroscopy. *ACS Photonics* **2020**, *7*, 36.

(7) Rodriguez, M.; Furse, C.; Shumaker-Parry, J. S.; Blair, S. Scaling the response of nanocrescent antennas into the ultraviolet. *ACS Photonics* **2014**, *1*, 496.

(8) Brown, J. M.; Davies, S. G. Chemical asymmetric synthesis. *Nature* **1989**, *342*, 631.

(9) Wang, Y.; Han, Q.; Zhang, Q.; Huang, Y.; Guo, L.; Fu, Y. Chiral recognition of penicillamine enantiomers based on a vancomycin membrane electrode. *Anal. Methods* **2013**, *5*, 5579.

(10) Budau, M.; Hancu, G.; Rusu, A.; Carcu-Dobrin, M.; Muntean, D. L. Chirality of modern antidepressants: An overview. *Adv. Pharm. Bull.* **2017**, *7* (4), 495.

(11) Micsonai, A.; Wien, F.; Kernya, L.; Lee, Y.-H.; Goto, Y.; Refregiers, M.; Kardos, J. Accurate secondary structure prediction and fold recognition for circular dichroism spectroscopy. *Proc. Natl. Acad. Sci. U. S. A.* **2015**, *112* (24), E3095.

(12) Green, D. W.; Lee, J. M.; Kim, E. J.; Lee, D. J.; Jung, H. S. Chiral biomaterials: From molecular design to regenerative medicine. *Adv. Mater. Interfaces* **2016**, *3*, 1500411.

(13) Clark, B. D.; Jacobson, C. R.; Lou, M.; Yang, J.; Zhou, L.; Gottheim, S.; DeSantis, C. J.; Nordlander, P.; Halas, N. J. Aluminum nanorods. *Nano Lett.* **2018**, *18*, 1234.

(14) Davis, M. S.; Zhu, W.; Lee, J. K.; Lezec, H. J.; Agrawal, A. Microscopic origin of the chiroptical response of optical media. *Science Advances* **2019**, *5*, eaav8262.

(15) Barriel, O. A. Mueller matrix polarimetry of anisotropic chiral media. Ph.D. Thesis, Universitat de Barcelona, 2010.

(16) Yin, X.; Schäferling, M.; Metzger, B.; Giessen, H. Interpreting chiral nanophotonic spectra: The plasmonic Born-Kuhn model. *Nano Lett.* **2013**, *13*, 6238.

(17) Fedotov, V. A.; Mladyonov, P. L.; Prosvirnin, S. L.; Rogacheva, A. V.; Chen, Y.; Zheludev, N. I. Asymmetric propagation of electromagnetic waves through a planar chiral structure. *Phys. Rev. Lett.* **2006**, *97*, 167401.

(18) Wang, M.; Gompf, B.; Dressel, M.; Destouches, N.; Berrier, A. Pure circular dichroism by curved rows of plasmonic nanoparticles. *Opt. Mater. Express* **2018**, *8*, 1515.

(19) McPeak, K. M.; van Engers, C. D.; Bianchi, S.; Rossinelli, A.; Poulikakos, L. V.; Bernard, L.; Herrmann, S.; Kim, D. K.; Burger, S.; Blome, M.; Jayanti, S. V.; Norris, D. J. Ultraviolet plasmonic chirality from colloidal aluminum nanoparticles exhibiting charge-selective protein detection. *Adv. Mater.* **2015**, *27*, 6244.

(20) Jeong, H. H.; Mark, A. G.; Fischer, P. Magnesium plasmonics for UV applications and chiral sensing. *Chem. Commun.* **2016**, *52*, 12179.

(21) Gutiérrez, Y.; de la Osa, R. A.; Ortiz, D.; Saiz, J. M.; González, F.; Moreno, F. Plasmonics in the ultraviolet with aluminum, gallium, magnesium, and rhodium. *Appl. Sci.* **2018**, *8*, 64.

(22) Sanz, J. M.; Ortiz, D.; Alcaraz de la Osa, R.; Saiz, J. M.; Gonzalez, F.; Brown, A. S.; Losurdo, M.; Everitt, H. O.; Moreno, F. UV plasmonic behavior of various metal nanoparticles in the near- and far-field regimes: Geometry and substrate effects. *J. Phys. Chem. C* **2013**, *117*, 19606.

(23) McClain, M. J.; Schlather, A. E.; Ringe, E.; King, N. S.; Liu, L.; Manjavacas, A.; Knight, M. W.; Kumar, I.; Whitmire, K. H.; Everitt, H. O.; Nordlander, P.; Halas, N. J. Aluminum nanocrystals. *Nano Lett.* **2015**, *15*, 2751.

(24) Gérard, D.; Gray, S. K. Aluminum plasmonics. *J. Phys. D: Appl. Phys.* **2015**, *48*, 184001.

(25) Knight, M. W.; King, N. S.; Liu, L.; Everitt, H. O.; Nordlander, P.; Halas, N. J. Aluminum for plasmonics. *ACS Nano* **2014**, *8*, 834.

(26) Chipman, R. A. Mueller Matrices. Polarimetry. In *Handbook of optics, Vol. 1: Geometrical and Physical Optics, Polarized Light, Components and Instruments*, 3rd ed.; Bass, M., Mahajan, V. N.; McGraw-Hill, 2010.

(27) Collins, J. T.; Kuppe, C.; Hooper, D. C.; Sibilia, C.; Centini, M.; Valev, V. K. Chirality and Chiroptical Effects in Metal Nanostructures: Fundamentals and Current Trends. *Adv. Opt. Mater.* **2017**, *5*, 1700182.

(28) Najafabadi, A. F.; Pakizeh, T. Analytical chiroptics of 2D and 3D nanoantennas. *ACS Photonics* **2017**, *4*, 1447.

(29) Eftekhari, F.; Davis, T. J. Strong chiral optical response from planar arrays of subwavelength metallic structures supporting surface plasmon resonances. *Phys. Rev. B: Condens. Matter Mater. Phys.* **2012**, *86*, 075428.

(30) Svirko, Y. P.; Zheludev, N. I. *Polarization of Light in Nonlinear Optics*; Wiley-VCH: New York, 1998.